Improved functional stability of a coarse-grained Ti-50.8 at.% Ni shape memory alloy achieved by precipitation on dislocation networks

Xiebin Wang[a,*], Ze Pu[a], Qin Yang[b], Shuke Huang[b], Zuocheng Wang[a,*], Sergey Kustov[c,d] and Jan Van Humbeeck[e]

[a]Key Laboratory for Liquid-Solid Structural Evolution and Processing of Materials (Ministry of Education), Shandong University, Jingshi Road 17923, Jinan 250061, China.

[b]Institute of Machinery Manufacturing Technology, China Academy of Engineering Physics, Mianyang 621900, China.

[c]Departament de Física, Universitat de les Illes Balears, Cra Valldemossa km 7.5, Palma de Mallorca E07122, Spain.

[d]ITMO University, Kronverkskiy av. 49, St. Petersburg 197101, Russia.

[e]Department of Materials Engineering, University of Leuven (KU Leuven), Kasteelpark Arenberg 44 bus 2450, Heverlee B3001, Belgium.

*Corresponding author: Tel.: +86 531 883 92621, Email: wangxiebin@sdu.edu.cn (X. Wang);

*Corresponding author: Tel.: +86 531 883 92621, Email: zcwang@sdu.edu.cn (Z. Wang).

Abstract

In this work, a new process is developed to improve the functional stability of Ni-rich NiTi alloys. Repetitive temperature- and stress-induced phase transformation is first conducted to generate dislocation networks in the grain interior. Dislocations serve as nucleation sites for Ni_4Ti_3 nanoprecipitates, which are formed after subsequent low-temperature (523 K) aging. With the presence of dislocations, a homogeneous distribution of nanoprecipitates in the grains is expected, enhancing the strength of the NiTi matrix and resisting plastic deformation during the martensitic transformation. As a result, an improved functional stability of NiTi alloys is achieved.

Keywords: Shape memory alloy (SMA), NiTi, precipitation, dislocations, functional stability.

Near equi-atomic NiTi shape memory alloys, which show excellent shape memory effect and superelasticity, are one of the most promising shape memory materials for practical applications [1-3]. During service, the NiTi devices normally undergo cyclic phase transformation between a B2 structured austenite (A) phase and a B19' structured martensite (M) phase [2]. The B2/B19' interface mismatch during transformation leads to generation of dislocations and plastic strain [4-12]. The irreversible plastic strain accumulates during cyclic phase transformation, resulting in degradation of functional properties (i.e. functional fatigue) [6,8,13]. Therefore, suppressing the plastic deformation by means of enhancing the strength of NiTi matrix is essential to reduce the accumulation of irreversible plastic strain and thus to improve the functional stability of NiTi alloys. Among all existing methods for strengthening metallic materials, grain refinement and precipitation hardening have been widely addressed as efficient approaches to improve the functional stability of NiTi alloys [14-18].

Many studies on the functional performance of ultrafine-grained NiTi alloys have shown that the functional stability could be remarkably improved by refining the grains to less than 100 nm [7,11,15,17-19], but extra-fine grains with the diameter <50 nm suppress the B19' martensite transformation [20,21], resulting in the change of the stress-strain response from superelasticity to linear-elasticity [19,22]. NiTi alloys with nano-sized grains are normally produced through severe plastic deformation (e.g. cold drawing [15], high-pressure torsion [23], equal-channel angular extrusion [24], repetitive cold rolling [25]) followed by an annealing treatment [15,22]. The main challenge is to maintain the grain size within a certain

range, due to the high ductility (tensile strain up to 50% [26]), rapid work hardening, high strength and high toughness associated with NiTi alloys [27].

Precipitation of Ni_4Ti_3 particles is an alternative efficient method to improve the strength of the matrix and the functional stability of Ni-rich NiTi alloys [14,16,28,29]. The precipitates are normally introduced by aging after high temperature solution treatment [1], which gives rise to large grains (several tens of microns). The large grains result in the heterogeneous distribution of Ni_4Ti_3 particles between grain boundary region and grain interior [30-34], which undermines the precipitation hardening effect. Moreover, the inhomogeneous distribution of Ni_4Ti_3 precipitates also disturbs the transformation sequence, leading to the appearance of multiple-stage transformation [1,31-35]. In our previous work [16,30,36], we revealed that grain size concomitant with aging could influence significantly the phase transformation behavior and functional properties. Low-temperature aging of Ni-rich NiTi alloys with small grains (e.g. 1.7 um [16,36]) leads to the homogeneous distribution of Ni_4Ti_3 particles, and the disappearance of multi-stage transformation. More importantly, the functional stability benefits remarkably from the homogeneously distributed Ni_4Ti_3 nanoprecipitates [16].

As discussed above, refined grains seem to be critical to improve the functional stability of NiTi alloys. However, in this work, we propose a new approach to enhance the functional stability of coarse-grained NiTi alloys. We first generate dislocations in the grain interior by repetitive phase transformation. Many studies have revealed that dislocations are introduced in NiTi grains during either thermally induced or stress-induced A↔M transformation [4,37-39]. Afterwards, low-temperature aging treatment is conducted to introduce

nanoprecipitates. According to the classical nucleation concept of solid-solid phase transformations, dislocations could act as the heterogeneous nucleation sites for precipitation [40]. As a result, a homogeneous distribution of Ni_4Ti_3 nanoprecipitates is expected, and thus the improvement of functional stability could be achieved through precipitation hardening.

A cold rolled Ti-50.8 at.% Ni plate with the thickness of 0.5 mm was used in this study. The as-received plates were annealed at 973 K for 2 h and water quenched at room temperature, followed by: (a) 120 thermal cycles between liquid nitrogen and boiling water (thermal-cycled sample); (b) 10 cycles of loading (up to 9.5%)-unloading (stress-cycled sample). Afterwards, the annealed sample, the thermal-cycled sample and the stress-cycled sample are subjected to an aging treatment at 523 K for 48 h to introduce Ni_4Ti_3 nanoprecipitates [36]. The microstructure of the as-annealed, thermal- and stress-cycled samples was characterized by means of electron backscatter diffraction (EBSD), transmission Kikuchi diffraction (TKD) and transmission electron microcopy (TEM). Both EBSD and TKD tests were performed using the Bruker QUANTAX system on a TESCAN MIRA3 microscope equipped with the e^-Flash^{HR} EBSD detector and OPTIMUS^{TM} TKD detector. TEM study was conducted using a FEI Titan Themis 80-300 instrument operating at an accelerating voltage of 300 kV. The surface for EBSD measurement, which is parallel to the rolling plane, was prepared by electro-polishing in a solution of 21 vol.% perchloric acid and 79 vol.% acetic acid at room temperature. The samples for both TKD and TEM observations were prepared using a Gatan 691 precision ion polishing system. The transformation behavior was characterized by differential scanning calorimetry (DSC) in a NETZSCH DSC 214 Polyma calorimeter with a cooling/heating rate of 10

K min^{-1}. The stability of superelasticity was characterized using a MTS tensile testing machine with a constant strain rate of 1.67×10^{-4} s^{-1}.

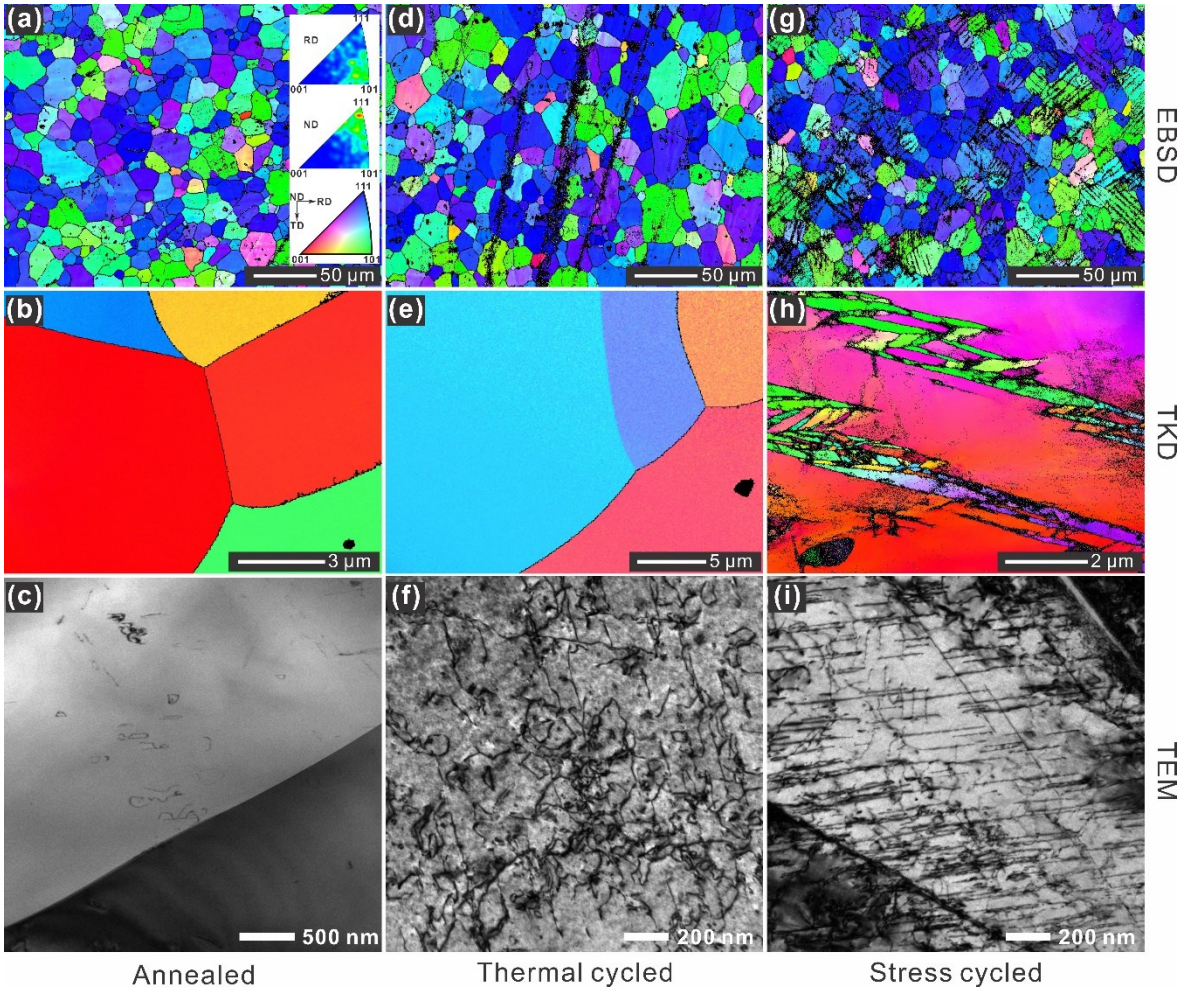

Figure 1. The microstructure of the cold rolled Ti-50.8 at.% Ni plate after annealing at 973 K for 2 h (a, b, c), and of the annealed samples after 120 thermal cycles (i.e. the thermal-cycled sample, d, e, f) or 10 stress cycles (i.e. the stress-cycled sample, g, h, i), as captured by electron backscatter diffraction (EBSD, a, d, g), transmission Kikuchi diffraction (TKD, b, e, h) and transmission electron microscopy (TEM) bright field image (c, f, i). The insets in (a) are the inverse pole figures with the reference to the rolling direction (RD) and normal direction (ND), respectively.

The annealed (973 K for 2 h) Ti-50.8 at.% Ni sample shows fully recrystallized equiaxed grains with an average grain size of 12 μm, as revealed in Fig. 1a. The average grain size was manually determined using the line intercept method described by Sutou *et al*. [41]. The annealed sample shows a texture of (111)//<110>, as indicated by the inverse pole figures of RD (rolling direction) and ND (normal direction) in Fig. 1a. According to the TKD results (Fig. 1b), the grains are surrounded by high angle grain boundaries and do not contain any obvious substructures. TEM observations (Fig. 1c) indicate very low dislocation density after annealing.

The microstructure of the thermal-cycled sample is shown in Fig. 1d-1f. No obvious microstructural difference with the annealed sample is revealed by means of EBSD and TKD. However, high density of tangled dislocations are observed by TEM (Fig. 1f). The dislocations are introduced by repetitive phase transformation between austenite and martensite, as frequently reported in previous studies [1,4,39].

The EBSD image in Fig. 1g reveals the traces of plastic deformation in the stress-cycled sample (i.e. the annealed sample subjected to 10 loading-unloading cycles), but the grain size remains essentially the same as in the annealed sample (Fig. 1a). The plastic strain accumulates rapidly in the annealed sample during superelastic cycling (Fig. 3a). Fine grains with high angle boundaries and irregular morphology are revealed by TKD in local areas (Fig 1h), indicating that the repetitive stress-induced transformations give rise to the grain refinement effect, as previously reported by Bowers et al. [42]. TEM observations (Fig. 1i) evidence significant dislocation activity during stress cycling.

As discussed above, dislocations networks are successfully introduced in the grain interior by repetitive phase transformation, either thermally or stress induced transformation, but the grain size remains essentially unchanged.

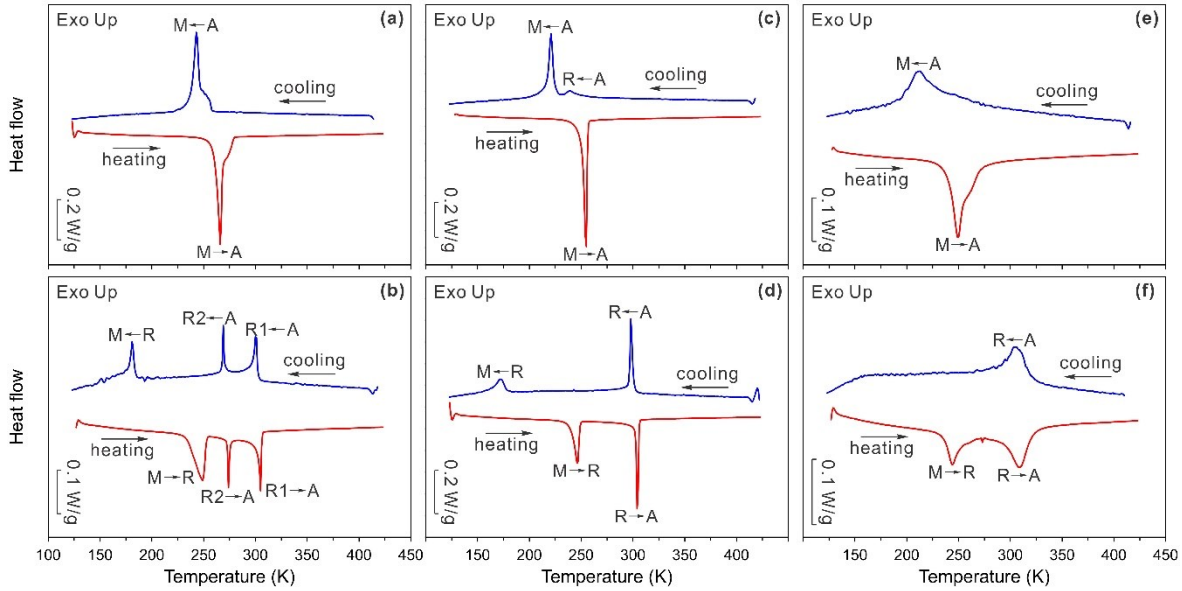

Figure 2. Transformation behavior, as detected by DSC, of the cold rolled Ti-50.8 at.% Ni plates after the following thermomechanical treatments: (i) annealing at 973 K for 2 h (a), directly followed by aging at 523 K for 48 h (b); (ii) annealing at 973 K for 2 h, followed by 120 thermal cycles between 373 K and liquid nitrogen temperature (c) and afterwards subjected to aging at 523 K for 48 h (d); (iii) annealing at 973 K for 2 h, followed by 10 stress cycles of loading up to 9.5% and unloading (e), and afterwards subjected to aging at 523 K for 48 h (f).

The annealed (973 K for 2 h) Ti-50.8 at.% sample shows a one stage A↔M transformation with the martensite transformation peak temperature (M_P) at 243 K (Fig. 2a). Two-stage R-phase transformation is observed in the annealed sample after aging at 523 K for 48 h (Fig. 2b). As discussed in our previous work [16,30,36], in the samples with large grains (e.g. average grain size >5.6 μm [30]), the two-stage R-phase transformation originates from the

inhomogeneous distribution of Ni_4Ti_3 precipitates between the grain boundary region and the grain interior. Therefore, the appearance of two-stage R-phase indicates the inhomogeneous distribution of Ni_4Ti_3 particles after aging in the annealed sample, which has an average grain size of 12 μm.

A→R→M transformation with M_P at 221 K is observed in the thermal-cycled sample, Fig. 2c. The appearance of the R-phase is due to the presence of dislocations (Fig. 1f) as discussed frequently in previous studies [1,43,44]. Figure 2d shows the transformation behavior of the thermal-cycled sample after aging at 523 K for 48 h. The two-stage R-phase transformation is absent, as compared with the sample, which did not undergo thermal cycling before aging treatment (Fig. 2b). We have shown that the disappearance of the two-stage R-phase transformation is indicative of the homogeneous distribution of Ni_4Ti_3 particles in the grains [30,31]. As shown in Fig. 1, the thermal-cycled sample has similar grain size as the as-annealed sample. Therefore, based on the evolution of the phase transformation behavior, we could conclude that the presence of dislocations in grain interior assists the precipitation of Ni_4Ti_3 particles, leading to their homogeneous distribution in the coarse-grained NiTi alloys.

Figures 2e and 2f show similar results for the stress-cycled sample. Without aging treatment, the stress-cycled sample demonstrates a one-stage A↔M transformation. The broad transformation peak is due to the plastic deformation during repetitive loading-unloading process. According to Fig. 2f, the stress-cycled sample subjected to aging also shows the A→R→M transformation during cooling. During forward transformation, only A→R transformation peak is detected by DSC, since the R→M transformation spreads over a wide temperature range. The reverse M→R transformation peak is clearly detected during heating

(Fig. 2f). It is worth noting that besides the effect of dislocations, the fine grain structure (Fig. 1h) also promotes the homogeneous distribution of Ni_4Ti_3 particles.

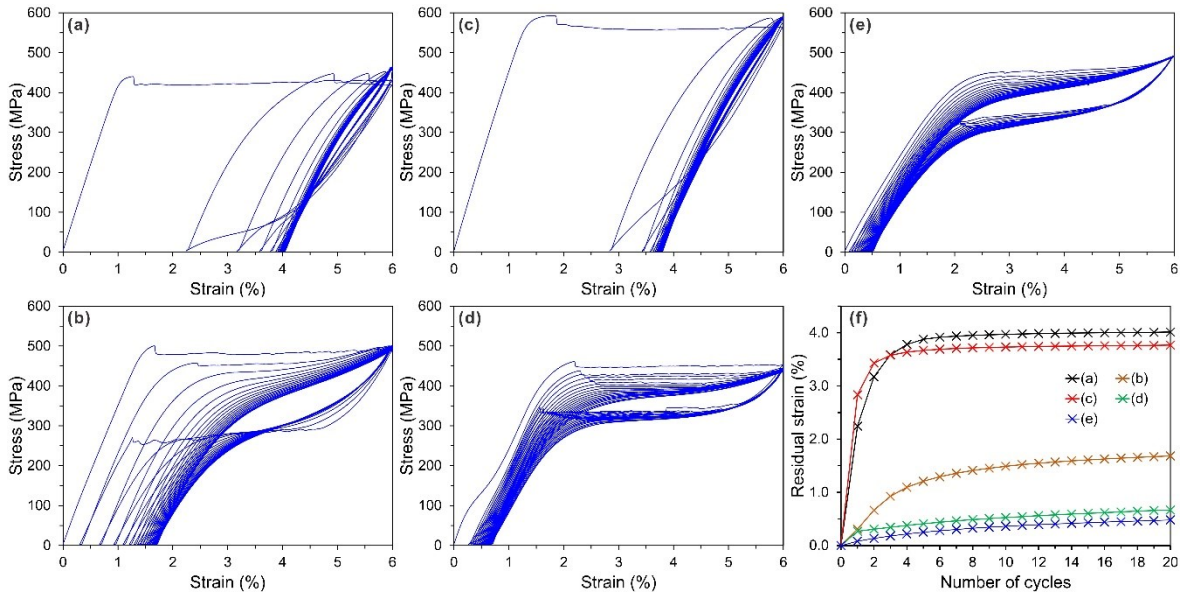

Figure 3. Room temperature superelastic cycling curves of the cold rolled Ti-50.8 at.% Ni plates after the following thermomechanical treatments: (i) annealing at 973 K for 2 h (a), directly followed by aging at 523 K for 48 h (b); (ii) annealing at 973 K for 2 h, followed by 120 thermal cycles between 373 K and liquid nitrogen temperature (c), and afterwards subjected to aging at 523 K for 48 h (d); (iii) annealing at 973 K for 2h, followed by 10 stress cycles of loading up to 9.5 % and unloading (i.e. panel a), and afterwards subjected to aging at 523 K for 48 h (e). Panel (f) summarizes the residual strain after each loading-unloading cycle. The data are taken from (a)-(e).

Figure 3 represents the stability of superelasticity of the annealed sample, thermal-cycled and stress-cycled samples, both before and after aging treatment. The residual irrecoverable strain of the annealed sample accumulates rapidly during the initial loading-unloading cycles, as shown in Fig. 3a. Although aging treatment (523 K, 48 h) improves the superelasticity of

the annealed sample, a large irrecoverable strain of 1.7% remains after 20 loading-unloading cycles (Fig. 3b).

Figure 3c shows the stability of superelasticity of the thermal-cycled sample. As compared with the annealed sample (Fig. 3a), the superelasticity barely benefits from the presence of dislocation networks, which are introduced by repetitive thermally induced A↔M transformation. Large irrecoverable strains of 2.8% and 3.8% are observed after 1 and 20 loading-unloading cycles, respectively (Fig. 3f). Figure 3d indicates that the stability of superelasticity of the thermal-cycled sample improves remarkably after aging treatment (523 K, 48 h). The irrecoverable strain is reduced to only 0.7% after 20 loading-unloading cycles, as indicated in Fig. 3f. It is worth noting that the irrecoverable strain also includes the strain caused by the R-phase transformation, as evidenced by the shoulder observed in the first loading cycle (Fig. 3d). Figure 3e demonstrates a significant improvement of the superelastic performance in the stress-cycled sample after aging at 523 K for 48 h. The irrecoverable strain is 0.5% after 20 loading-unloading cycles, as shown in Fig. 3f. The results in Fig. 3 indicate that low-temperature aging after repetitive A↔M phase transformation improves significantly the functional stability of coarse-grained NiTi alloys.

The above results indicate that dislocation networks, created by repetitive phase transformation, could indeed affect significantly the aging microstructure. This modification is clearly reflected in the phase transformation behavior (Fig. 2) and functional properties (Fig. 3). As discussed in our previous work [30,31], aging of large-grained samples (grain size above ca. 6 μm [30]) creates inhomogeneous distribution of Ni_4Ti_3 nanoprecipitates between grain boundary region and grain interior, path (a)→(b) in Fig.4, since grain boundaries assist the

precipitation of second phase particles [33,45]. Consequently, the two-stage A→R transformation is observed, exemplified by Fig. 2b. Data in Fig. 3b prove that superelastic cycling of samples with such inhomogeneous distribution of Ni_4Ti_3 nanoprecipitates is accompanied by significant plastic strains.

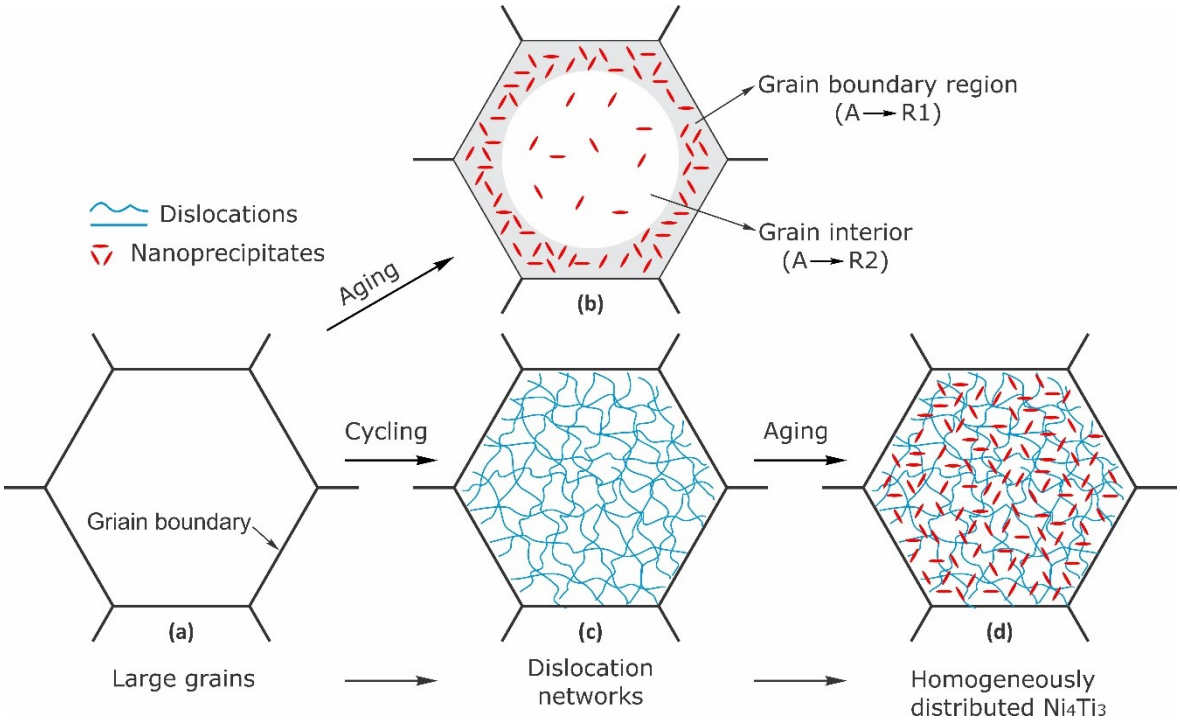

Figure 4. Schematic illustration on the influence of dislocation networks on the distribution of nanoprecipitates.

Dislocation networks are introduced in the grain interior by repetitive A↔M transformation, either thermally- or stress-induced ones, path (a)→(c) in Fig.4. In addition to grain boundaries, the dislocations also act as the nucleation sites for Ni_4Ti_3 precipitates, leading to the increased density of precipitation in the grain interior after aging (path (c)→(d) in Fig. 4), and thus to the homogeneous distribution of nanoprecipitates over the grains. The homogeneous

distribution of nanoprecipitates results in the disappearance of multiple stage martensitic transformation (Fig. 2) and improved functional stability during cyclic loading (Fig. 3).

In summary, we demonstrate that the functional stability of the coarse-grained Ni-rich NiTi alloys could be improved significantly by an approach featured with repetitive phase transformation followed by low-temperature aging treatment. The process includes two consecutive steps: (i) creation of dislocation networks in the grain interior by repetitive temperature- or stress-induced martensite transformation; (ii) homogeneous precipitation, assisted by dislocations, of Ni_4Ti_3 nanoparticles inside coarse grains, during subsequent low-temperature aging. The functional stability benefits remarkably from the homogeneous distribution of nanoprecipitates. It should be specially emphasized that the suggested method suits NiTi structures with complex shapes and large grains, for instance, those fabricated by additive manufacturing.

Acknowledgement

This work was funded by the National Key R&D Program of China (Grant No.: 2018YFB1105100), Shandong Provincial Natural Science Foundation, China (Grant No.: ZR2018QEM001), China Postdoctoral Science Foundation (Grant No.: 2017M622195), the Young Scholars Program of Shandong University (Grant No. 2018WLJH24), the Fundamental Research Funds of Shandong University, and the Research Foundation Flanders (FWO, Grant No.: G.0366.15N). The financial support from the Spanish Ministerio de Economía y Competitividad, Project MAT2014-56116-C04-01-R and by the Ministry of Education and Science of the Russian Federation, goszadanie No. 3.1421.2017/4.6 is also acknowledged. We

would like to thank Dr. B.J. Yu (Bruker, Shanghai) for conducting the EBSD and TKD measurements.

References:

[1] K. Otsuka, X. Ren, Prog. Mater. Sci. 50 (2005) 511.

[2] K. Yamauchi, I. Ohkata, K. Tsuchiya, S. Miyazaki, Shape Memory and Superelastic Alloys: Technologies and Applications, Woodhead Publishing, Cambridge, UK., 2011.

[3] L. Lecce, A. Concilio, Shape Memory Alloy Engineering for Aerospace, Structural and Biomedical Applications, Butterworth-Heinemann, Oxford, UK, 2015.

[4] J. Zhang, C. Somsen, T. Simon, X. Ding, S. Hou, S. Ren, X. Ren, G. Eggeler, K. Otsuka, J. Sun, Acta Mater. 60 (2012) 1999.

[5] M.L. Bowers, X. Chen, M. De Graef, P.M. Anderson, M.J. Mills, Scripta Mater. 78-79 (2014) 69.

[6] P. Chowdhury, H. Sehitoglu, Prog. Mater. Sci. 85 (2017) 1.

[7] R. Delville, B. Malard, J. Pilch, P. Sittner, D. Schryvers, Int. J. Plast. 27 (2011) 282.

[8] Y. Gao, L. Casalena, M.L. Bowers, R.D. Noebe, M.J. Mills, Y. Wang, Acta Mater. 126 (2017) 389.

[9] H.M. Paranjape, M.L. Bowers, M.J. Mills, P.M. Anderson, Acta Mater. 132 (2017) 444.

[10] A.W. Richards, R.A. Lebensohn, K. Bhattacharya, Acta Mater. 61 (2013) 4384.

[11] P. Sedmak, P. Sittner, J. Pilch, C. Curfs, Acta Mater. 94 (2015) 257.

[12] T. Simon, A. Kröger, C. Somsen, A. Dlouhy, G. Eggeler, Acta Mater. 58 (2010) 1850.

[13] G. Eggeler, E. Hornbogen, A. Yawny, A. Heckmann, M. Wagner, Mater. Sci. Eng. A 378 (2004) 24.

[14] J.I. Kim, S. Miyazaki, Acta Mater. 53 (2005) 4545.

[15] R. Delville, B. Malard, J. Pilch, P. Sittner, D. Schryvers, Acta Mater. 58 (2010) 4503.

[16] X. Wang, S. Kustov, K. Li, D. Schryvers, B. Verlinden, J. Van Humbeeck, Acta Mater. 82 (2015) 224.

[17] A. Ahadi, Q. Sun, Acta Mater. 90 (2015) 272.

[18] A. Yawny, M. Sade, G. Eggeler, Z. Metallkd. 96 (2005) 608.

[19] B. Malard, J. Pilch, P. Sittner, V. Gartnerova, R. Delville, D. Schryvers, C. Curfs, Funct. Mater. Lett. 2 (2009) 45.

[20] T. Waitz, K. Tsuchiya, T. Antretter, F.D. Fischer, MRS Bull. 34 (2009) 814.

[21] T. Waitz, V. Kazykhanov, H.P. Karnthaler, Acta Mater. 52 (2004) 137.

[22] A. Ahadi, Q. Sun, Acta Mater. 76 (2014) 186.

[23] M. Peterlechner, T. Waitz, H.P. Karnthaler, Scripta Mater. 60 (2009) 1137.

[24] B. Kockar, I. Karaman, J.I. Kim, Y. Chumlyakov, J. Sharp, C.-J. Yu, Acta Mater. 56 (2008) 3630.

[25] M. Peterlechner, J. Bokeloh, G. Wilde, T. Waitz, Acta Mater. 58 (2010) 6637.

[26] S. Miyazaki, Y. Kohiyama, K. Otsuka, T.W. Duerig, Mater. Sci. Forum 56-58 (1990) 765.

[27] M. Elahinia, N.S. Moghaddam, M.T. Andani, A. Amerinatanzi, B.A. Bimber, R.F. Hamilton, Prog. Mater. Sci. 83 (2016) 630.

[28] H.E. Karaca, S.M. Saghaian, G. Ded, H. Tobe, B. Basaran, H.J. Maier, R.D. Noebe, Y. Chumlyakov, Acta Mater. 61 (2013) 7422.

[29] S. Miyazaki, T. Imai, Y. Igo, K. Otsuka, Metall. Trans. A 17 (1986) 115.

[30] X. Wang, C. Li, B. Verlinden, J. Van Humbeeck, Scripta Mater. 69 (2013) 545.

[31] X. Wang, B. Verlinden, S. Kustov, Funct. Mater. Lett. 10 (2017) 1740004.

[32] B. Karbakhsh Ravari, S. Farjami, M. Nishida, Acta Mater. 69 (2014) 17.

[33] Y. Zhou, J. Zhang, G. Fan, X. Ding, J. Sun, X. Ren, K. Otsuka, Acta Mater. 53 (2005) 5365.

[34] J. Khalil-Allafi, A. Dlouhy, G. Eggeler, Acta Mater. 50 (2002) 4255.

[35] J.I. Kim, Y. Liu, S. Miyazaki, Acta Mater. 52 (2004) 487.

[36] X. Wang, K. Li, D. Schryvers, B. Verlinden, J. Van Humbeeck, Scripta Mater. 72-73 (2014) 21.

[37] K. Gall, H.J. Maier, Acta Mater. 50 (2002) 4643.

[38] J. Hurley, A.M. Ortega, J. Lechniak, K. Gall, H.J. Maier, Z. Metallkd. 94 (2003) 547.

[39] A.R. Pelton, G.H. Huang, P. Moine, R. Sinclair, Mater. Sci. Eng. A 532 (2012) 130.

[40] D.A. Porter, K.E. Easterling, Phase Transformations in Metals and Alloys, second ed., Springer-Sicence+Business Media, B.V. Berlin, 1992.

[41] Y. Sutou, T. Omori, K. Yamauchi, N. Ono, R. Kainuma, K. Ishida, Acta Mater. 53 (2005) 4121.

[42] M.L. Bowers, Y. Gao, L. Yang, D.J. Gaydosh, M. De Graef, R.D. Noebe, Y. Wang, M.J. Mills, Acta Mater. 91 (2015) 318.

[43] S. Miyazaki, Shap. Mem. Superelasticity 3 (2017) 279.

[44] X. Wang, B. Verlinden, J. Van Humbeeck, Intermetallics 62 (2015) 43.

[45] G. Fan, W. Chen, S. Yang, J. Zhu, X. Ren, K. Otsuka, Acta Mater. 52 (2004) 4351.